

Fission properties of superheavy nuclei for r -process calculations

Samuel A. Giuliani,^{1,*} Gabriel Martínez-Pinedo,^{2,1,†} and Luis M. Robledo^{3,‡}

¹*Institut für Kernphysik (Theoriezentrum), Technische Universität Darmstadt,
Schlossgartenstraße 2, 64289 Darmstadt, Germany*

²*GSI Helmholtzzentrum für Schwerionenforschung, Planckstraße 1, 64291 Darmstadt, Germany*

³*Departamento de Física Teórica, Universidad Autónoma de Madrid, E-28049 Madrid, Spain*

(Dated: July 16, 2022)

We computed a new set of static fission properties suited for r -process calculations. The potential energy surfaces and collective inertias of 3640 nuclei in the superheavy region are obtained from Self-Consistent Mean-Field calculations using the Barcelona-Catania-Paris-Madrid energy density functional. The fission path is computed as a function of the quadrupole moment by minimizing the potential energy and exploring octupole and hexadecapole deformations. The spontaneous fission lifetimes are evaluated employing different schemes for the collective inertias and vibrational energy corrections. This allows to explore the sensitivity of the lifetimes to those quantities together with the collective ground state energy along the superheavy landscape. We computed neutron induced stellar reaction rates relevant for r -process nucleosynthesis using the statistical approach and study the impact of collective inertias. The competition between different reaction channels including neutron induced rates, spontaneous fission and alpha decay is discussed for typical r -process conditions.

I. INTRODUCTION

The theoretical description of the fission process is one of the most challenging and fascinating problems in nuclear physics. The competition between the long-range Coulomb repulsion and the short-range strong interaction drives the evolution of the nucleus from the ground state to the scission point. Furthermore, they produce quantum mechanical shell effects that allow for the stability of superheavy elements (SH) in the heaviest regions of the nuclear landscape. Probably one of the most interesting applications of fission concerns the r -process nucleosynthesis of superheavy elements. In scenarios with high neutron densities, like for instance the dynamical ejecta of neutron stars mergers, the competition between rapid neutron captures and beta decays of seed nuclei leads to the synthesis of superheavy elements. The r -process path proceeds towards regions of unstable nuclei that undergo fission, recycling the material to lighter fission products [1–3]. In these conditions, fission plays a relevant role not only by modifying the final shape of the r -process abundances [4, 5], but also in providing a mechanism to achieve a robust r -process [6]. Besides astrophysical applications, the stability of the nucleus against fission is also crucial for the experimental synthesis of superheavy nuclei achieved in laboratories all around the world during the past years [7–10] and for energy production in nuclear reactors.

Nowadays, the main nuclear structure models describing the spontaneous fission (SF) are the microscopic-macroscopic (MicMac) and the self-consistent mean-field (SCMF) models (see ref. [11] for a recent review on fission properties of SH nuclei covering MicMac and SCMF

models). The MicMac description pioneered the modern modeling of the fission process in the late sixties and since then several studies have been successfully applied in systematic calculations of superheavy nuclei. One of the main advantages of this method is the calculation of the potential energy surface in multidimensional spaces using up to five collective degrees of freedom for systematic calculations, providing an accurate description of multiple fission paths (see, e.g. refs. [12–14] for recent calculations). On the other hand, 20 years ago fission calculations based on self-consistent methods with effective interactions entered the scene, proposing an alternative scheme built on a more microscopic approach. Starting from an effective energy density functional (EDF), the constrained Hartree-Fock (HF) and Hartree-Fock-Bogoliubov (HFB) theories permit the calculation of the fission properties rooted on more microscopic input. In the last years, several studies explored the capability of the EDF theory to reproduce the experimental fission data using either Skyrme [15–21], Gogny [22–28] or relativistic interactions [29] (see [30] for a complete review).

The main objective of this paper is to present the fission properties of r -process nuclei obtained with the Barcelona-Catania-Paris-Madrid (BCPM) EDF [31]. As already pointed out in [32], nowadays only few global calculations suited for r -process calculations are publicly available. This work is designed to provide a new set of fission properties based in the SCMF model covering the whole superheavy landscape and including nuclei with an odd number of protons and/or neutrons. The main advantage of the EDF theory is that allows the computation of both the potential energy surface and the collective inertias from a unique and microscopic footing, providing a robust framework for the calculation of spontaneous fission lifetimes, fission barrier heights and isomer excitation energies. The paper is outlined as follows. In Sec. II we briefly introduce the method used in the calculation of the potential energy surface and spontaneous

* giuliani@theorie.ikp.physik.tu-darmstadt.de

† g.martinez@gsi.de

‡ luis.robledo@uam.es

fission lifetimes. In Sec. III we summarize the results of our calculations. We start discussing the benchmark of BCPM against the experimental data in Sec. III A. The systematic of fission barriers and spontaneous fission lifetimes is discussed in Sec. III B and Sec. III C. Sec. III D is devoted to discuss the competition between α -decay and spontaneous fission and in Sec. III E the discussion is extended to neutron induced rates of relevance to r -process. Finally, in Sec. IV we summarize our results and outline the future perspectives.

II. METHODS

In this paper fission is described within the Self-Consistent Mean-Field (SCMF) approach [33] following the traditional HFB theory with constraining operators as described in Ref. [34]. For completeness we will summarize here the general computational scheme and point out the uncertainties arising from our method.

In order to reduce the computational cost, axial symmetry has been preserved in all the calculations. The impact of releasing this restriction has been object of several recent studies (see e.g. [19, 20, 26]), where it has been shown that triaxiality can reduce the inner fission barrier height of actinides up to 2–3 MeV. However, we would like to point here that the role of triaxiality in fission is still the subject of discussion since some recent calculations showed that axial symmetry can be fully restored in dynamic calculations of the fission process [24, 35, 36]. Moreover, this reduction of the fission barrier is compensated by an increase of the collective inertias and therefore the impact of releasing this symmetry is expected to be small in the calculation of fission lifetimes.

Due to the preservation of axial symmetry, the mean-value of the multipole operators, $\langle Q_{\mu\nu} \rangle = 0$ for all $\nu \neq 0$. In order to explore the impact of octupole and hexadecapole deformations, as well as asymmetric fission, reflection symmetry is allowed to break at any stage of the calculations. The basis quantum numbers are restricted by the condition:

$$2n_{\perp} + |m| + \frac{n_z}{q} \leq N^{\max}. \quad (1)$$

All the calculations were carried with $N^{\max} = 17$ and $q = 3/2$. The parameter q , somehow related to the ratio of HO frequencies ω_{\perp}/ω_z , is used to modulate the number of quantum states along the z direction. The value used favors more shells in the z direction which is the one relevant to fission. Once the number of quanta in each direction is fixed, the basis only depends on the oscillator lengths b_z and b_{\perp} . To diminish the impact of the limited basis size on the binding energies, it is mandatory to carefully optimize the oscillator length parameters for each value of the constrained quadrupole moment considered in the calculation. The optimization is carried out automatically using the gradient method to find the minimum of the HFB energy as a function of the two oscillator length variables b_{\perp} and b_z . The gradient of the

energy with respect to b_{\perp} and b_z is computed numerically using a three point formula for the numerical derivative. This is a costly procedure as each evaluation of the energy $E(b_{\perp}, b_z)$ requires the solution of the corresponding HFB equation. In order to decrease the computational cost, the oscillator lengths b_{\perp} and b_z characterizing the HO basis were minimized only for a selected set of nuclei at each value of the quadrupole deformation. For the other nuclei, the oscillator lengths of the nearby nuclei were used. The suitability of this simplification is demonstrated by the smooth dependence of b_{\perp} and b_z with mass number for fixed values of the quadrupole moment. The HFB equations were solved using a second-order gradient method, which provides a fast convergence and allows for an arbitrary generalization of the numbers of constraints [37]. The main advantage of the computational scheme described above is that it has already been applied to several fission calculations using either the Gogny or the BCPM interactions [22, 26–28, 34, 38], and its capability to describe the fission process is well constrained.

We have used the last version of the BCPM functional recently proposed to describe the physics of finite nuclei [31]. This functional has also proved to perform well in a series of calculations of fission properties including inner fission barrier heights, excitation energy of fission isomers, outer barrier heights, spontaneous fission lifetimes, etc. The idea behind the explicit form of the BCPM functional is to use a simple polynomial in the density to fit the energy per particle in both symmetric and neutron nuclear matter as obtained with state of the art many body techniques and realistic nuclear interactions. The polynomial so obtained is used verbatim in finite nuclei but using the density of the finite nucleus instead. A standard contact spin-orbit term is added to reproduce magic numbers. Surface effects are considered by means of a finite range gaussian interaction acting only in the direct channel. The Coulomb interaction is taken, as in many other calculations, exactly in the direct channel. The exchange Coulomb field is replaced by the Slater approximation and the repulsive contribution of the Coulomb interaction to the pairing channel is neglected. For the pairing interaction, a density dependent pairing interaction has been used. One of the distinctive characteristics of the functional is its inclusion of the rotational energy correction (see below) to compute the ground state binding energy. The rotational correction is also used in the fitting protocol in spite of the fact that its inclusion produces some artifacts near magic or semimagic nuclei [31]. They are a direct consequence of computing the rotational correction after variation and disappear if beyond mean field effects like configuration mixing of quadrupole deformed shapes is taken into account. Unfortunately, the artifacts in the rotational correction lead to spurious peaks in both the S_n , S_{2n} and related quantities near magic or semimagic nuclei, which can produce unphysical abundances in r -process calculations. For this reason, we have decided to remove the rotational correction in the evaluation of

one and two neutron separation energies. The impact of this prescription in the S_n rms for $Z > 84$ is small increasing its value from 0.28 MeV to 0.36 MeV. However, the rotational correction is maintained in fission barrier calculations as the artifacts do not appear in the relevant regions of the path to fission.

A. Spontaneous fission lifetimes, fission barriers and collective inertias

The spontaneous fission lifetimes (t_{sf}) are computed following the semiclassical Wentzel-Kramers-Brillouin (WKB) theory [39]:

$$t_{\text{sf}} = \frac{\ln 2}{nP} = 2.86 \times 10^{-21} (1 + \exp(2S)), \quad (2)$$

being n the number of assaults of the nucleus on the fission barrier per unit time [40]. The penetration probability P can be written in terms of the integral action S computed along the fission path $L(Q_{20})$ between the classical turning points a and b

$$S(L) = \int_a^b dQ_{20} \sqrt{2\mathcal{M}(Q_{20})[\mathcal{V}(Q_{20}) - (E_0 + E_{\text{GS}})]}, \quad (3)$$

where the fission path $L(Q_{20})$ is obtained by minimizing the potential energy (so-called static approach). From Eq. (3) it turns out that the theoretical description of the SF process is based in three main ingredients: the collective inertias $\mathcal{M}(Q_{20})$, the effective potential energy $\mathcal{V}(Q_{20})$ and the energy of the collective ground state E_0 . The effective potential energy $\mathcal{V}(Q_{20})$ is obtained by subtracting the vibrational and rotational zero-point energies from the total HFB energy:

$$\mathcal{V}(Q_{20}) = E_{\text{HFB}}(Q_{20}) - \epsilon_{\text{vib}}(Q_{20}) - \epsilon_{\text{rot}}(Q_{20}). \quad (4)$$

The HFB energy E_{HFB} is defined as the expectation value of the Routhian with constraining operators:

$$\hat{\mathcal{H}} = \hat{\mathcal{H}}_{\text{HFB}} + \sum_{\nu=1,2} \lambda_{\nu} \hat{Q}_{\nu 0} + \sum_{\tau=p,n} \lambda_{\tau} \hat{N}_{\tau}, \quad (5)$$

being $\hat{\mathcal{H}}_{\text{HFB}}$ the HFB Hamiltonian, $\hat{N}_p(\hat{N}_n)$ the proton (neutron) number operator, λ_i the Lagrange multipliers and Q_{10} the center-of-mass constraint preventing spurious solutions arising from center-of-mass motion. The rotational energy correction $\epsilon_{\text{rot}}(Q_{20})$ is related to the restoration of the rotational symmetry and is computed in terms of the Yoccoz moments of inertia using the phenomenological approach of Ref. [41]. Finally, the vibrational energy correction $\epsilon_{\text{vib}}(Q_{20})$ takes into account for quantal fluctuations in the collective degree of freedom Q_{20} . The lower panels of Fig. 1 show the different contributions of Eq. (4) to the Potential Energy Surface (PES) in four different nuclei. Clearly the major reduction to $\mathcal{V}(Q_{20})$ comes from the rotational correction $\epsilon_{\text{rot}}(Q_{20})$, while the vibrational correction $\epsilon_{\text{vib}}(Q_{20})$ produces a smaller, yet not constant, shift. From these plots

it is clear that both the rotational and zero-point energy corrections introduced in Eq. (4) can modify the final height of the fission barriers B_I and B_{II} and the isomer excitation energy E_{II} . The second ingredient needed for the calculation of the SF lifetimes are the collective inertias $\mathcal{M}(Q_{20})$. In the present work we evaluated $\mathcal{M}(Q_{20})$ (and $\epsilon_{\text{rot}}(Q_{20})$) following two different schemes within the perturbative cranking approximation: the Adiabatic Time-Dependent HFB theory (ATDHFB) [42] and the Gaussian Overlap Approximation to the Generator Coordinate Method (GOA-GCM) [43]

$$\mathcal{M}_{\text{ATDHFB}}(Q_{20}) = \frac{M_{-3}}{2(M_{-1})^2}, \quad (6)$$

$$\mathcal{M}_{\text{GOAGCM}}(Q_{20}) = \frac{(M_{-2})^2}{2(M_{-1})^3}. \quad (7)$$

The energy-weighted momentum $M_{(-n)}(Q_{20})$ of the quadrupole generating field can be expressed in terms of the two-quasiparticle excitations $|\alpha\beta\rangle$:

$$M_{(-n)}(Q_{20}) = \sum_{\alpha>\beta} \frac{|\langle\alpha\beta|Q_{20}|0\rangle|^2}{(E_{\alpha} + E_{\beta})^n}, \quad (8)$$

being $E_{\alpha} + E_{\beta}$ the excitation energy neglecting the quasiparticle-quasiparticle interaction. The ATDHFB scheme has the advantage that naturally includes the time-odd response of the system to small perturbations in the deformation. In the simple case of a center-of-mass motion of the nucleus, the inclusion of the time-odd momenta allows the ATDHFB scheme to predict the exact collective inertia as the mass of the nucleus [43]. By contrast the GCM scheme does not include the time-odd response of the system and the inertias are underestimated unless time-odd momenta coordinates are used as collective degree of freedom. However, since translation and fission are collective phenomena involving different dynamics this argument cannot be used for claiming a superiority of the ATDHFB scheme over the GCM one.

For consistency, the $\epsilon_{\text{vib}}(Q_{20})$ terms are evaluated in either the ATDHFB or the GCM approaches according to the collective inertias:

$$\epsilon_{\text{vib}}^{\text{ATDHFB}}(Q_{20}) = \frac{G(Q_{20})}{\mathcal{M}_{\text{ATDHFB}}}, \quad (9)$$

$$\epsilon_{\text{vib}}^{\text{GOAGCM}}(Q_{20}) = \frac{G(Q_{20})}{\mathcal{M}_{\text{GOAGCM}}}, \quad (10)$$

where $G(Q_{20})$ is the overlap width between two configurations with similar quadrupole deformations:

$$G(Q_{20}) = \frac{M_{-2}}{2(M_{-1})^2}. \quad (11)$$

We noticed that in several calculations of fission cross sections the collective inertias are obtained from the semiempirical formula $\mu = 0.054A^{5/3}$ MeV $^{-1}$, being β_{20} the collective variable of the action integral (3). This semiempirical expression was obtained in order to reproduce experimental data in the actinide region using a

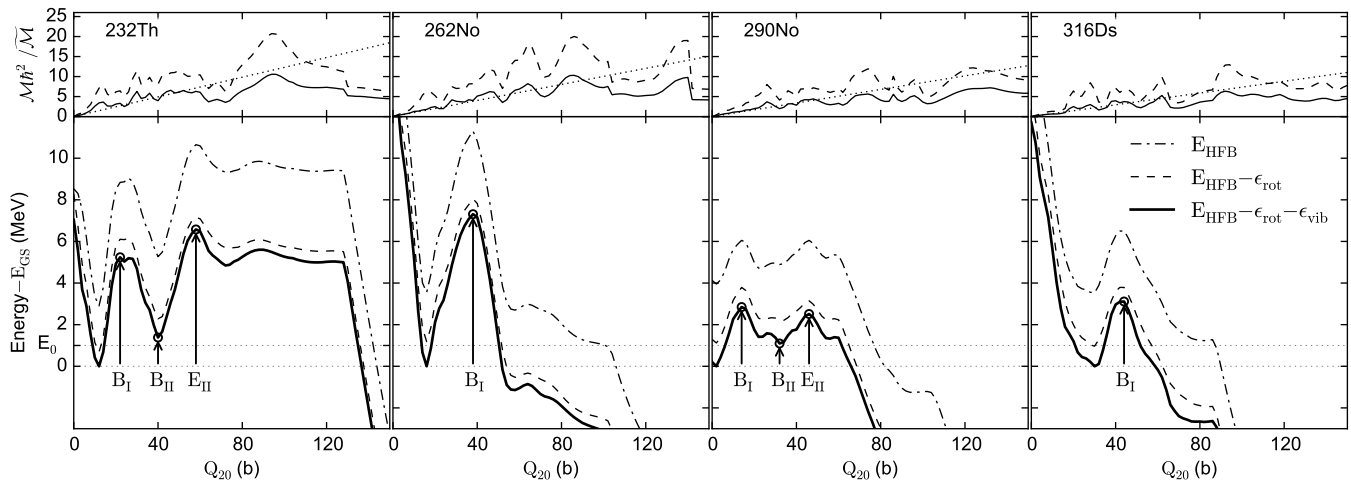


FIG. 1. Collective fission properties of ^{232}Th , ^{262}No , ^{290}No and ^{316}Ds as a function of the quadrupole moment. Lower panels show different contributions to the potential energy surface $\mathcal{V}(Q_{20})$ of Eq. (4). Upper panels show collective inertias $\mathcal{M}(Q_{20})$ computed with the ATDHFB (dashed line), GCM (solid line) and semiempirical inertia formula (dotted line), renormalized to the semiclassical inertia $\tilde{\mathcal{M}}(Q_{20}) = m_n/4Q_{20}$.

simplified prescription for the fission barriers [44]. The validity of μ for heavier nuclei and/or when different barriers to those of Moretto and Swiatecki are used, is rather uncertain and not fully tested. We decided therefore to compare the spontaneous fission lifetimes obtained with this semiempirical expression with the results obtained using the ATDHFB and GOA-GCM approaches. Since the action integral is invariant under uniform scaling, and $\beta_{20} = \frac{\sqrt{20}\pi}{5.4} \frac{Q_{20}}{r^2}$ with $r = 1.2A^{1/3}$ fm, we have that:

$$\mathcal{M}_{\text{SEMP}} = \mu \left(\frac{d\beta_{20}}{dQ_{20}} \right)^2 = \frac{0.065}{A^{5/3}} \text{ MeV}^{-1} \text{ fm}^{-4}. \quad (12)$$

Fig. 2 shows the region of the nuclear landscape explored in this work. Nuclei for which the BCPM interaction predicts a strong oblate deformation of the ground-state ($\beta_{20} \leq -0.1$) are depicted with solid circles. These nuclei are supposed to undergo fission through a triaxial path and should be computed with an explicit breaking of the K quantum number. Since a triaxial code for the BCPM interaction is not available we treated these nuclei computing the axial path, but it is necessary to keep in mind that predictions of the fission properties for these nuclei are less reliable.

B. Odd nuclei

The estimation of nuclear properties of nuclei with an odd number of protons and/or neutrons is a critical issue in SCMF models. A self-consistent solution obtained on the same footing as even-even nuclei is rather expensive from the computational point of view and therefore difficult to be implemented in systematic calculations (see [46] and references therein for a general comparison between different approaches). For this reason, a good

compromise in systematic calculations is to use a phenomenological approach aimed to reproduce the experimental bulk nuclear properties of odd-even and odd-odd nuclei.

In this work, we computed the bulk nuclear properties of odd nuclei in the region $84 \leq Z \leq 120$ and $118 \leq N \leq 250$ using the Perturbative Nucleon Addition Method (PNAM) [47]. By adopting the PNAM method BCPM maintains the same level of accuracy achieved for even-even nuclei in the calculation of nuclear binding energies and fission properties when odd-even and odd-odd nuclei are included. Namely, the BCPM EDF without rotational correction reproduces the experimental binding energies of even-even nuclei [45] with a rms deviation of 2.67 MeV, that decreases down to 2.37 MeV when odd nuclei computed with the PNAM are included. But the agreement of the absolute binding energies can be misleading since the relevant quantities for r -process calculations are the neutron separation energy entering in the estimation of the neutron capture cross section. With the BCPM EDF the neutron separation energies S_n are reproduced with a rms deviation of 0.30 MeV for even-even nuclei and 0.36 MeV including odd nuclei. The robustness of these results gives us the confidence to explore the whole superheavy landscape using the BCPM EDF in combination with the PNAM.

Fig. 3 shows the two-neutron separation energies S_{2n} predicted by BCPM for nuclei with $84 \leq Z \leq 120$ and the comparison with HFB21 [48] and FRDM [49] models. Jumps in the two-neutron separation energies (commonly defined as energy gaps $\Delta_{2n} = S_{2n}(Z, N) - S_{2n}(Z, N+2)$) are usually associated with the presence of shell closures and during the r -process nucleosynthesis result in accumulation of matter. For example, for nuclei with $Z \sim 96$ the predicted neutron magic number $N = 184$ plays an important role in the production of the heaviest elements during the r -process nucleosynthesis in neutron

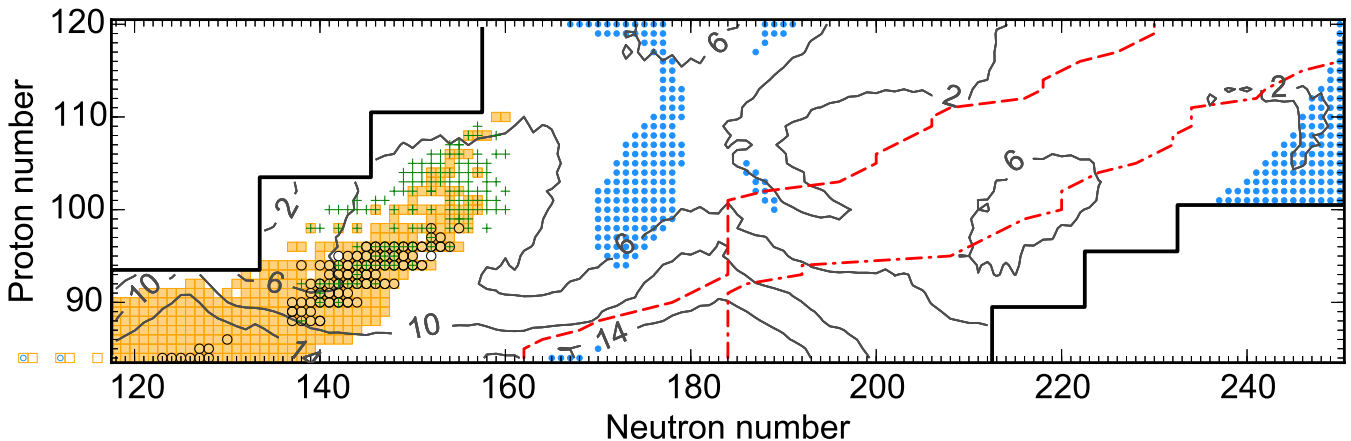


FIG. 2. Region of the nuclear landscape explored in this work. Nuclei present in the AME2012 mass table evaluation [45] are depicted with orange squares. Nuclei with experimentally measured fission barriers and spontaneous fission lifetimes are marked with open circles and crosses, respectively. Nuclei for which the BCPM interaction predicts an oblate-deformed ground state are depicted with solid circles. Dashed and dot-dashed lines represent the heaviest isotope of each element with $S_n \gtrsim 2$ and $S_n \gtrsim 0$ MeV, respectively. Contour lines show the highest predicted fission barrier, in MeV.

star mergers, since it allows the accumulation of material around $A \sim 280$ [6]. Fig. 4 shows that BCPM predicts a higher energy gap compared to HFB17 and FRDM for nuclei with $N = 184$ that smoothly disappears with increasing proton number. As we will discuss in Sec. III B this disappearance may allow the r -path to proceed towards heavier nuclei if the fission barriers around ${}_{100}^{284}\text{Fm}$ are high enough.

For some nuclei BCPM predicts a potential energy surface with a vanishing fission barrier. For these nuclei a minimum energy cannot be defined and they are considered unstable, in the sense that after their production they will immediately decay by fission. They are followed by nuclei with a prolate ground state and depicted in Fig. 3 with a gap in the isotopic lines.

Regarding the collective inertias, we applied the same perturbative scheme used for even-even nuclei described in Sec. II A. This approach neglects the enhancement of collective inertias due to the quenching of pairing correlations in systems with unpaired nucleons, leading to a possible underestimation of spontaneous fission lifetimes of nuclei with an odd number of neutrons and/or protons.

III. RESULTS

A. Benchmarks

In Ref. [34] we studied the fission properties of the BCPM EDF for a reduced set of even-even nuclei and compared our results with experimental measurements. In this paper we present the extension of such calculations to the whole superheavy landscape including nuclei with an odd number of protons and/or neutrons in the region $84 \leq Z \leq 120$ and $118 \leq N \leq 250$.

In order to validate the theoretical predictions of the BCPM EDF, we compared our results of the barriers

heights and isomer excitation energies with the available experimental data of Bjørnholm and Lynn [50] and Capote *et al.* [51]. Whether the fission barriers can be considered a physical observable or not is still an argument of discussion in the community. Without entering in this discussion, we would like to point out that experimental fission barriers are extracted from fission cross sections measurements, assuming nuclear level densities and shapes of the potential energy surface predicted by theoretical models. The experimental values of the fission barriers are therefore model dependent, and consequently the comparison with theoretical values should be taken with a grain of salt.

Fig. 5 shows the BCPM predictions and the experimental data of the inner (B_I) and outer (B_{II}) fission barrier height and the isomer excitation energy (E_{II}). We found that BCPM reproduces the B_I , B_{II} and E_{II} experimental values of Bjørnholm and Lynn [50] with a rms deviation of 1.29, 0.81 and 1.22 MeV respectively. The discrepancies with the data set of Capote *et al.* [51] are slightly larger: 1.51 MeV for B_I and 0.97 MeV for B_{II} , while no data is available for E_{II} . The largest differences have been found in the Uranium, Plutonium, and Americium isotopes. For these nuclei BCPM predicts a clear increase of the three quantities with increasing neutron number, while experimental data shows an almost constant trend. In many cases the PNAM provides a good description of the odd-even staggering of the fission barriers within single isotopic chains, and the inclusion of odd nuclei does not substantially modify the agreement with experimental data.

The origin of the discrepancies may be different for the different quantities. In the case of the inner barrier height, the discrepancies are probably related to the preservation of axial symmetry. Triaxiality can reduce the inner fission barrier heights up to 2-3 MeV, improving the agreement with experimental data. Regarding the discrepancies of the outer fission barrier height and

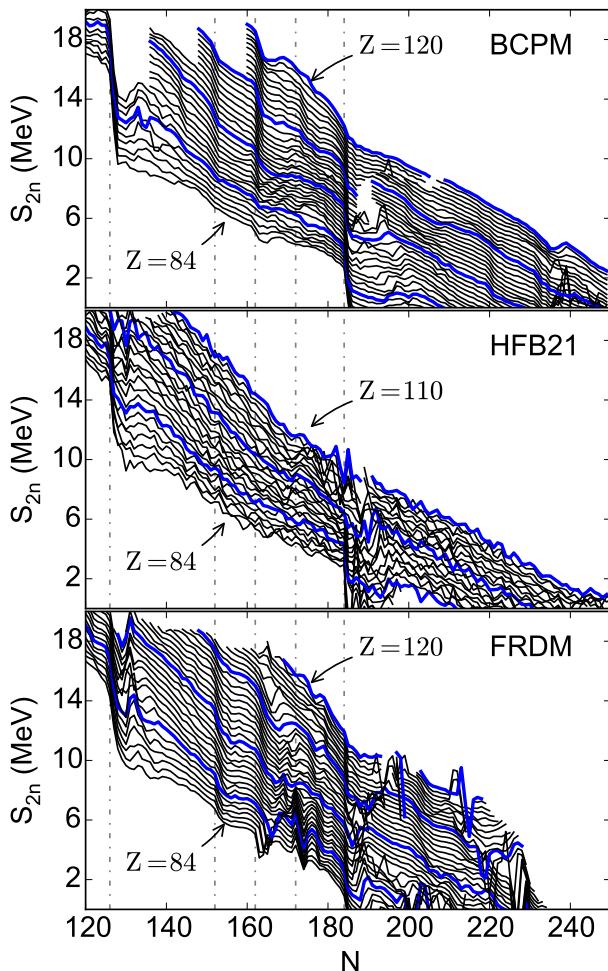


FIG. 3. Predicted two-neutron separation energies in MeV for nuclei with $84 \leq Z \leq 120$ as a function of neutron number for three different models: BCPM (upper panel), HFB21 (middle panel) and FRDM (lower panel). Isotopic chains are connected by solid lines. Nuclei with a proton number equal to 90, 100, 110 and 120 are depicted with blue thick lines.

isomer excitation energy, the discussion is more involved. In principle, the evolution of the energy as a function of the quadrupole moment plotted in Fig. 1 is driven by the competition between the decreasing surface energy and the increasing Coulomb repulsion of the protons in the nucleus. However, at larger deformations both shell effects and pairing correlations may strongly influence the shape of the barriers. Therefore, one way to improve the agreement with experimental data may rely in a refit of the BCPM EDF, allowing for a more flexible pairing interaction and surface energy contribution.

The other main spontaneous fission observable besides the barrier height is the spontaneous fission lifetime t_{sf} , that can be experimentally measured without any model assumption. This observable can be estimated with logarithmic precision within the semiclassical WKB formalism described in Sec. II A and is closely related to the penetration probability, an important ingredient in the evaluation of fission cross section.

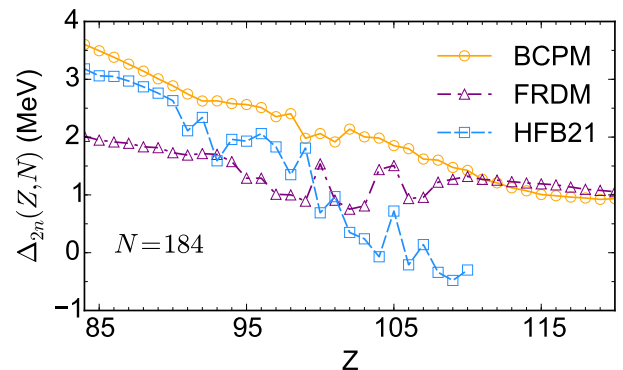


FIG. 4. Energy gap $\Delta_{2n} = S_{2n}(Z, N) - S_{2n}(Z, N + 2)$ in MeV for nuclei with $N = 184$ as a function of proton number predicted by BCPM (open circles), FRDM (triangles) and HFB21 (squares).

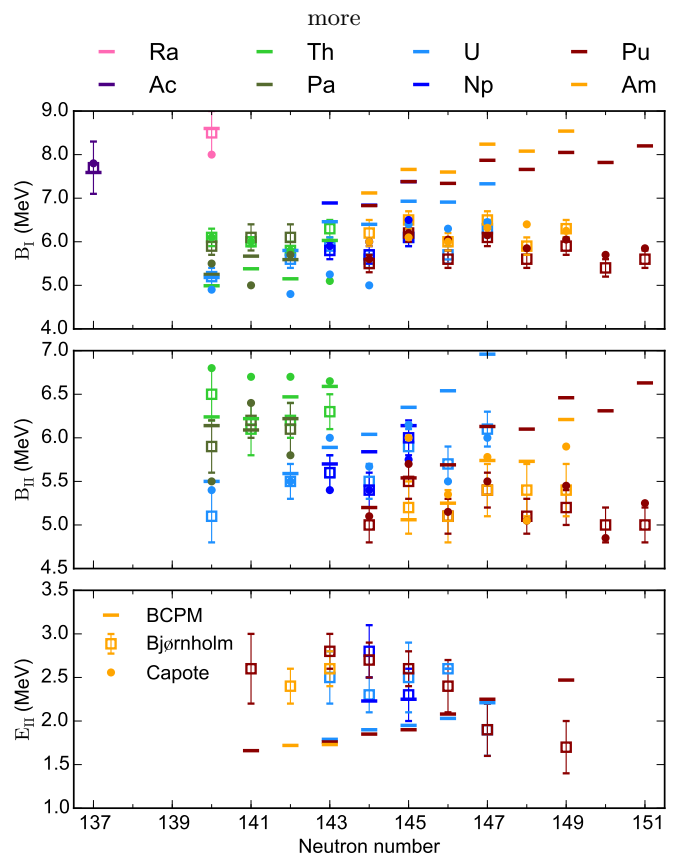


FIG. 5. Inner fission barrier height B_I (upper panel), outer fission barrier height B_{II} (middle panel) and isomer excitation energy E_{II} (lower panel) of eight isotopes computed with BCPM (lines) and compared with experimental data of Bjørnholm [50] (open squares) and Capote [51] (circles).

We computed the t_{sf} using the three different collective inertia schemes: ATDHFB (Eq. (6)), GCM (Eq. (7)) and the semiempirical formula (Eq. (12)). Fig. 6 shows the comparison between our results and the experimental data extracted from Ref. [52, 53]. Both the ATDHFB and GCM microscopic schemes predict larger SF lifetimes

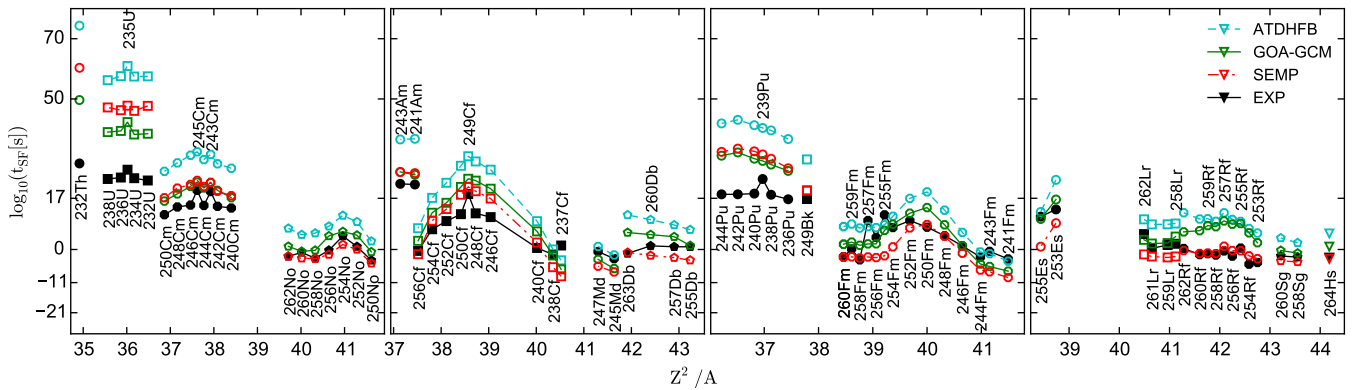


FIG. 6. Experimental spontaneous fission lifetimes [52, 53] (solid markers) are compared with BCPM predictions (open symbols) using different collective inertia schemes: ATDHFB (Eq. (6)), GOAGCM (Eq. (7)) and semiempirical formula (Eq. (12)). Nuclei are plotted as a function of the fissibility parameter Z^2/A and isotopic chains are connected by lines.

compared to the experimental data, while the semiempirical formula overestimates the t_{sf} of nuclei with $Z \leq 98$ and slightly underestimates the lifetimes of nuclei with $Z \geq 99$.

The spread among theoretical lifetimes and the discrepancy with experimental data are large for light actinides, while for heavier nuclei predictions become more accurate and precise. This convergence of theoretical calculations can be understood by looking at the fission barriers plotted in Fig. 1. The left panel shows the fission path of the nucleus ^{232}Th giving the largest difference between theoretical and experimental half-lives. This nucleus presents a broad fission barrier together with a large collective inertia, resulting in a large action integral $S(L)$ where variations in the collective inertias have a strong impact in the spontaneous fission lifetimes. On the other hand, the nucleus ^{262}No has a much shorter barrier with relatively small inertia between the classical turning points. This configuration reduces the value of the action integral and the impact of different collective inertia schemes in the absolute magnitude of t_{sf} , all giving a good prediction of the experimental value. For r -process nuclei where fission may play a relevant role, like ^{290}No and ^{316}Ds plotted in Fig. 1, the t_{sf} has to be relatively short. Therefore these nuclei must have a narrow and/or low fission barrier and small collective inertias, bringing to a level of precision in the estimation of the t_{sf} closer to the one obtained for the ^{262}No rather than the ^{232}Th .

For most of the isotopic chains the general trend of the spontaneous fission lifetimes is well reproduced by all the collective inertias schemes. Moreover, the odd-even staggering of the fission barriers is reflected in the lifetimes in a rather good agreement with experimental data. However it is important to notice that this staggering is more pronounced in the experimental t_{sf} , suggesting for a missing mechanism enhancing the collective inertias in these nuclei as discussed in Sec. II B.

The general overestimation of the spontaneous fission lifetimes in Fig. 9 suggests that both the fission barriers and the collective inertias are overestimated in our ap-

proach. While the discussion of the fission barriers has already been approached and can be related with the imposition of axial symmetry, the discussion regarding the collective inertias is more complicated.

On one hand, the overestimation of the spontaneous fission lifetimes can be related to lower pairing correlations that increase the collective inertias via smaller quasiparticle energies. As already suggested in [34], one could try to improve the agreement with experimental data by including the t_{sf} data in the fitting protocol of the pairing interaction. Conversely, one should also consider the approximations employed in our computational scheme. In principle the Perturbative Cranking Approximation (PCA) used in our calculations is expected to underestimate the collective inertias. A recent study [54] shows that a more “exact” calculation of the mass tensor involving the exact numerical differentiation of the energy kernels (also known as Non-Perturbative Cranking Approximation) leads to larger collective inertias. In our case such kind of calculation will clearly worsen the agreement with experimental data. This apparent contradiction arises from the fact that in our model we are exploring only one degree of freedom, namely the quadrupole mass operator Q_{20} as it is sketched in Fig. 1. Therefore, the overestimation of the spontaneous fission lifetimes can be cured by computing the fission path by means of the minimum action principle in a multidimensional space. As it was studied in several recent papers [35, 36, 38], the dynamic approach has a strong impact in the penetration probability and it can drastically reduce the t_{sf} improving the agreement with experimental data. However such method requires for multidimensional calculations exploring different collective variables, that unfortunately is too demanding for being applied in systematic calculations like those presented in this paper.

For this reason we propose a renormalization of the collective inertias aimed to take into account for all those effects neglected in the static one-dimensional picture and improve the agreement with experimental data. Since the t_{sf} can vary in many orders of magnitude, we follow

\mathcal{M}	\bar{R}_τ	σ_τ
ATDHFB	11.583	6.447
GCM	4.691	4.236
SEMP	2.036	6.126
ATDHFB-r	-0.007	3.403
GCM-r	-0.006	3.339
SEMP-r	0.004	5.231

TABLE I. Target performances (\bar{R}_τ) and variances (σ_τ) of the spontaneous fission lifetimes obtained with ATDHFB, GCM and semiempirical collective inertias described in Sec. II A. The lower table shows the results obtained by multiplying the collective inertias by a renormalization factor (0.497 for ATDHFB, 0.731 for GCM and 0.868 for SEMP). Experimental values extracted from Ref. [52, 53].

the prescription of Ref. [55] and define

$$R_\tau = \log \left(\frac{t_{\text{sf}}^{\text{BCPM}}}{t_{\text{sf}}^{\text{exp}}} \right). \quad (13)$$

The target performance \bar{R}_τ and the variance σ_τ are then obtained as:

$$\bar{R}_\tau = \frac{1}{N} \sum_{i=1}^N R_{\tau,i}, \quad (14)$$

$$\sigma_\tau = \frac{1}{N} \left(\sum_{i=1}^N (R_{\tau,i} - \bar{R}_\tau)^2 \right)^{1/2}, \quad (15)$$

being N the number of nuclei used in the benchmark. Comparing the logarithm of the ratio of theory to experiment we found that the target performance of the ATDHFB, GCM and semiempirical inertia schemes is 11.583, 4.691 and 2.036, respectively. Table I shows that by multiplying the ATDHFB, GCM and SEMP collective inertias by a factor 0.497, 0.731 and 0.868 respectively (labeled as ATDHFB-r, GCM-r and SEMP-r respectively), we sensibly improve the agreement of the predicted t_{sf} with experimental data. The main aim of the normalization is to reduce the action integral of light actinides (Th, U and Pu), where the high stability against the fission process leads to large values of the action integral and larger discrepancies with the experimental data. On the other hand, as we move towards heavier nuclei we would expect a general decrease of the fission stability and therefore a smaller impact of the renormalization in the absolute value of the fission lifetimes. The renormalization of the collective inertias shall be considered as an alternative to other approaches like, for instance, the renormalization of the fission barriers proposed in Ref. [16].

The results of the fission barrier height and the SF lifetimes presented in this section proved the capability of the BCPM+PNAM scheme to reproduce the experimental data. We consider this agreement rather satisfactory, specially taking into account that the BCPM EDF was fitted in order to reproduce the nuclear masses of the

AME2003 mass table [56] and it does not contain any information regarding the fission properties of superheavy nuclei.

B. Systematic of fission barriers

Fig. 7 shows the highest barrier predicted by the BCPM EDF for nuclei in the region $84 \leq Z \leq 120$ and $118 \leq N \leq 250$ and the comparison with the theoretical predictions of the FRLDM [13] and HFB-14 [16] nuclear models.

The general trend of fission barriers gives a crude estimation of the stability of nuclei against the fission process and reflects the impact of shell closures. BCPM predicts five different islands of local maximum placed around nuclei ${}_{84}^{210}\text{Po}$, ${}_{84}^{268}\text{Po}$, ${}_{100}^{250}\text{Fm}$, ${}_{102}^{320}\text{No}$ and ${}_{120}^{300}\text{Ubn}$. The increase of fission barriers around ${}_{84}^{210}\text{Po}$ and ${}_{84}^{268}\text{Po}$ is related with the presence of the neutron magic numbers $N = 126$ and $N = 184$, leading to spherical nuclei with fission barriers up to 24-25 MeV. These two islands are separated by prolate nuclei with fission barriers around 12 MeV and a group of slightly oblate nuclei around $Z/N = 86/176$. Regions around ${}_{100}^{250}\text{Fm}$ and ${}_{120}^{300}\text{Ubn}$ are usually referred as “peninsula of known nuclei” and “island of stability”, respectively. The peninsula is formed by prolate-deformed nuclei with fission barriers between 6 and 9 MeV and it extends up to $Z/N \approx 110/166$. On the other hand, nuclei in the island of stability are either oblate (for lower N) or spherical (higher N) with fission barriers around 7 MeV. The peninsula and the island are separated by a rather narrow region of prolate nuclei with $A \sim 280$ where the fission barriers decrease to 3-5 MeV. Finally, the region around ${}_{102}^{320}\text{No}$ is formed by strongly-deformed nuclei ($\beta_{20} \sim 0.25$) with barriers between 7 and 8 MeV. BCPM predicts a region of vanishing barriers around $Z/N = 116/208$ and for nuclei with $A \sim 292$ around $N \sim 188$. As discussed later, this region of vanishing barriers may play an important role for terminating the r -process via neutron induced fission.

For a complete comparison Fig. 7 shows the fission barriers predicted by two other models: the macroscopic-microscopic Finite Range Liquid Drop Model (FRLDM) [13] and the self-consistent mean field approach based on the HFB14 Skyrme parametrization [16]. Both models show a general trend of the fission barriers similar to the one obtained with the BCPM EDF, with two islands of larger fission barriers around $Z/N = 90/184$ and $Z/N = 100/150$. Moreover, all the models predict a region of vanishing barriers around $Z/N = 104/188$. BCPM tends to predict larger barriers compared to those obtained with FRLDM for nuclei with $Z \leq 100$ corresponding to the neutron magic number $N = 184$. On the other hand, FRLDM predicts larger barriers (up to 5 MeV) in the region around $Z/N = 112/178$. Comparing the results obtained with BCPM and HFB14, we found this two mean-field models predict similar maximum fission barrier heights. The rms deviation between both models is 1.03 MeV, while the de-

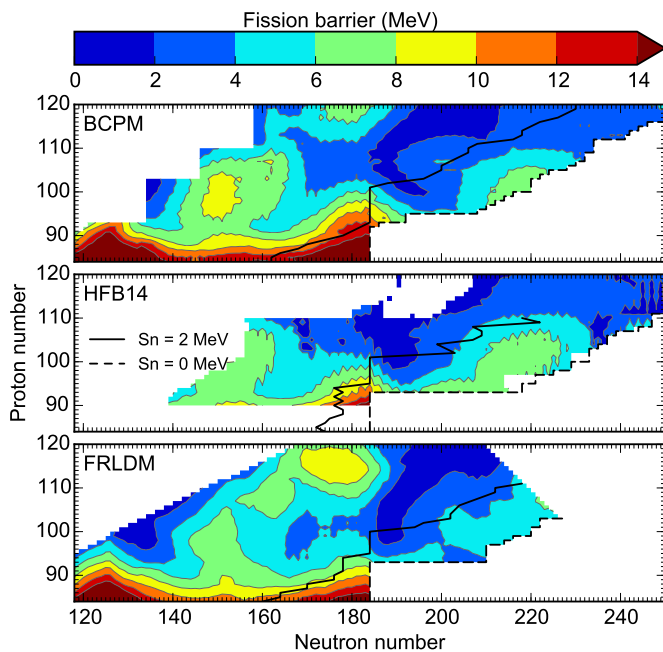


FIG. 7. Calculated fission barrier heights in MeV in the region $84 \leq Z \leq 120$ and $118 \leq N \leq 250$ for three different mass models: BCPM (this study, upper panel), HFB14 [16] (middle panel) and FRLDM [13] (lower panel). Drip lines are represented by dashed black lines. The solid black lines show the r -process path, given by the heaviest isotope of each nuclei with $S_n \geq 2$ MeV.

viation between BCPM and FRLDM is 2.31 MeV. The major differences between BCPM and HFB14 are found in neutron rich actinides where HFB14 predicts fission barriers larger by 2-3 MeV, and around $Z/N = 97/187$ and $106/196$ where BCPM barriers are roughly 2 MeV larger.

Another quantity of major interest for astrophysical calculations is the energy window for neutron-induced fission given as the difference between the highest fission barrier height and the neutron separation energy $B_f - S_n$. This quantity indicates whether the production of superheavy nuclei during the r -process can be inhibited by neutron-induced fission, recycling the material to lighter fission products. Fig. 8 shows the values of $B_f - S_n$ obtained with the BCPM EDF. In principle, an appropriate estimation of the r -process path would require a network calculation taking into account neutron captures, beta- decays and photodissociations. However, from simple arguments it is still possible to make a rough estimation of where the r -process path will be terminated by the neutron-induced fission. For typical astrophysical conditions in neutron star mergers, the r -process path is supposed to proceed along nuclei with constant neutron separation energy $S_n \sim 2-3$ MeV [57]. On the other hand, the excitation energy of a nucleus after capturing a neutron is given by the neutron separation energy. From these arguments one concludes that nuclei with $B_f - S_n \sim 2$ MeV will immediately fission after capturing a neutron [58, 59]. Fig. 8 shows how the r -process path is

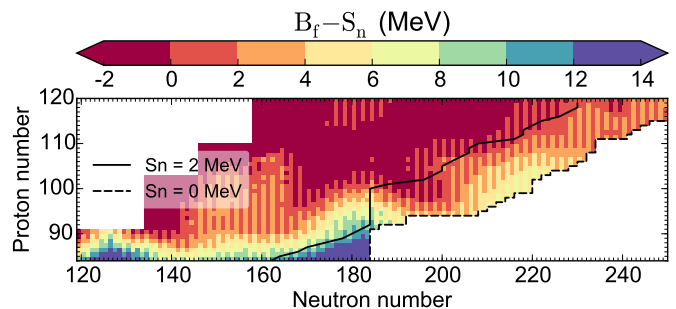


FIG. 8. Energy window for the neutron-induced fission $B_f - S_n$ computed with the BCPM EDF. The solid black line represents the r -process path, given by the heaviest isotope of each nuclei with $S_n \geq 2$ MeV. The drip line predicted by the BCPM EDF is represented by dashed line.

stacked along nuclei with $N = 184$ until $Z = 102$, where the disappearance of the jump in the neutron separation energy described in Sec. II B allows to overcome the waiting point. However, at this point the r -process path has already proceeded into the region of low fission barriers where $B_f - S_n$ drops below zero ($Z/N = 102/190$). Therefore, we may expect the r -process nucleosynthesis of superheavy nuclei to be terminated by the neutron induced fission in the region around $Z/N = 102/190$.

C. Systematic of fission lifetimes

The trend of the fission barriers gives only a rough hint of the stability of the nucleus against the fission process. As it was already explained in Sec. II A, the probability of the system to penetrate the fission barrier is determined by a complex process where several ingredients must be taken into account and it can not be solely determined by the height of the barrier. A more complete picture can be therefore obtained studying the trend of the spontaneous fission lifetimes and the contribution of the different terms entering in Eq. (3). In this section we will study the sensitivity of the spontaneous fission lifetimes to variations in the collective inertias $\mathcal{M}(Q_{20})$, the vibrational energy corrections $\epsilon_{\text{vib}}(Q_{20})$ and the collective ground state energy E_0 . Fig. 9 shows the t_{sf} obtained from Eq. (3) using the three different schemes of the collective inertias described in Sec. II A. For the ATDHFB and GCM schemes the vibrational energy corrections are consistently computed using Eq. (9) and (10). For the semiempirical inertias we arbitrarily choose the $\epsilon_{\text{vib}}^{\text{ATDHFB}}(Q_{20})$ scheme. Regarding the collective ground state energy, all the lifetimes were obtained with $E_0 = 0.5$ MeV. Due to the arbitrariness in the choice of these last two parameters, the second part of this section will be devoted to study the sensitivity of the lifetimes on ϵ_{vib} and E_0 .

From Fig. 9 it is possible to conclude that the trend of the spontaneous fission lifetimes resembles the general trend of the maximum fission barrier height plotted in

the upper panel of Fig. 7. This means that quantities like collective inertias and the shape of the barrier are responsible for local variations in the stability of the nucleus against the fission process. Nevertheless, the choice of the collective inertias scheme has a clear impact on the absolute value of the spontaneous fission lifetimes. For example, the semiempirical inertias predict a substantial larger amount of nuclei with $t_{\text{sf}} \lesssim 3$ s (marked as dotted region Fig. 9). This is the timescale at which the r -process operates from the onset of neutron captures till the exhaustion of all neutrons.

Due to the inclusion of the time-odd response of the nucleus to small perturbations of the deformation, the t_{sf} predicted by the ATDHFB scheme are systematically larger than the GCM ones and usually they are also larger than those obtained with the semiempirical scheme. There is only a small set of nuclei where the lifetimes predicted by GCM are larger than the ATDHFB ones. These nuclei correspond to the most extreme case of instability, with almost vanishing fission barrier and $t_{\text{sf}} \sim 10^{-21}$ s, where the rotational energy correction $\epsilon_{\text{rot}}(Q_{20})$ plays a leading role in determining the SF lifetimes. For nuclei with $Z \leq 96$ semiempirical lifetimes lie in between of the ATDHFB and the GCM lifetimes, while for nuclei with $Z > 96$ the semiempirical lifetimes become smaller than GCM ones.

The larger discrepancies among the different schemes are found in the region where the fission lifetimes are extremely high ($Z \lesssim 96$). As we already pointed out in Sec. III A, this is because the differences in the collective inertia are amplified by the large value of the action integral $S(L)$ entering in the exponential of the lifetimes t_{sf} . But due to the stability of these nuclei against the fission process their fission decay will not play a relevant role during the r -process nucleosynthesis.

Since we are interested in nuclei relevant for r -process calculations, in the following we will restrict the discussion to nuclei with $t_{\text{sf}} \leq 3$ s. For a more detailed comparison Fig. 10 shows the ratio of the lifetimes computed with different collective inertia schemes: ATDHFB to GCM (upper panel), ATDHFB to semiempirical inertias (middle panel) and GCM to semiempirical inertias (lower panel). The values showed in this plot correspond to the quantity

$$R_{\mathcal{M}_2}^{\mathcal{M}_1} = \log \left(\frac{t_{\text{sf}}(\mathcal{M}_1)}{t_{\text{sf}}(\mathcal{M}_2)} \right), \quad (16)$$

being $t_{\text{sf}}(\mathcal{M}_i)$ the spontaneous fission lifetime computed using the collective inertia \mathcal{M}_i . For these nuclei the average difference in the SF lifetimes using different inertias schemes is between one and three orders of magnitude, which in principle may be related also to the fact that theory only gives a logarithmic precision of the half-lives. The largest differences are found between the ATDHFB and semiempirical schemes in nuclei lying between the r -path and the neutron drip-line and around the shell closure $N = 184$. Since the former is a relevant region for r -process nucleosynthesis, such variations in the penetrability may have an impact in the final r -process abun-

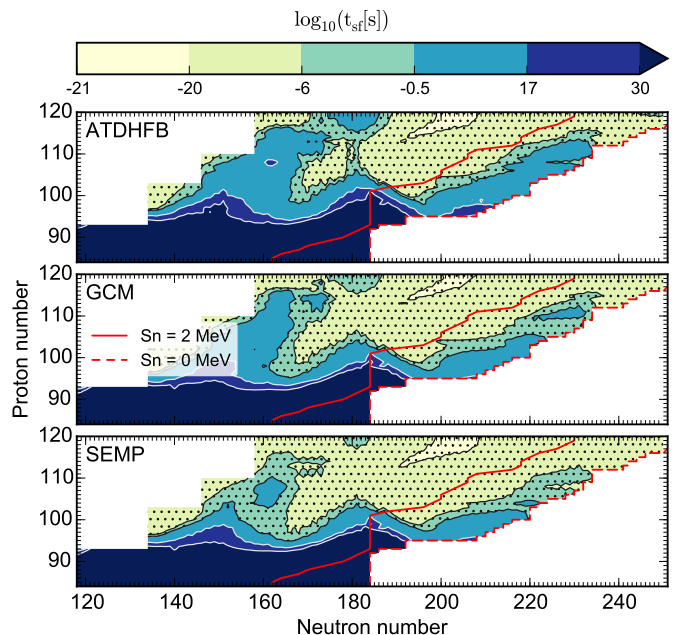


FIG. 9. Decimal logarithm of the spontaneous fission lifetimes (Eq. (2)) computed with the ATDHFB (Eq. (6), upper panel), GCM (Eq. (7), lower panel) and semiempirical (Eq. (12), lower panel) schemes. Dotted regions represent nuclei with $t_{\text{sf}} \leq 3$ s which may be relevant for r -process calculations. All the lifetimes were obtained with $E_0 = 0.5$ MeV.

dances.

Another source of uncertainty in the estimation of t_{sf} is the collective ground state energy E_0 . Fig. 11 shows the logarithm of the lifetimes ratio of 0.5 to 1.5 MeV computed with the ATDHFB, GCM and the semiempirical inertias. We found that for many nuclei the sensitivity of t_{sf} on E_0 is comparable to the sensitivity on the collective inertias. The reason is because nuclei plotted in Fig. 11 have relatively short barriers and usually with a complex shape presenting multiple humps, like in the case of the ^{290}No plotted in Fig. 1. As it was already extensively studied in Ref. [22], the presence of a second fission isomer increases the spontaneous fission lifetimes by several orders of magnitude. By increasing the E_0 to 1.5 MeV the isomer can be shifted below the ground-state energy of the nucleus, and therefore the lifetimes are strongly reduced since the third hump does not contribute anymore to the penetration probability.

We conclude this discussion showing the impact of the vibrational zero-point energy correction ϵ_{vib} on the spontaneous fission lifetimes. Fig. 12 shows the logarithm of the ratio of t_{sf} computed with the same semiempirical inertias and two different ϵ_{vib} calculations, obtained from the ATDHFB and GCM formalisms of Eqs. (9) and (10). We found that the t_{sf} computed with the ATDHFB ϵ_{vib} are usually between 1 and 2 orders of magnitude larger than the GCM ones, but variations induced by the zero-point energy correction are lower compared to the sensitivity of the lifetimes to different collective inertia schemes and collective ground-state energies.

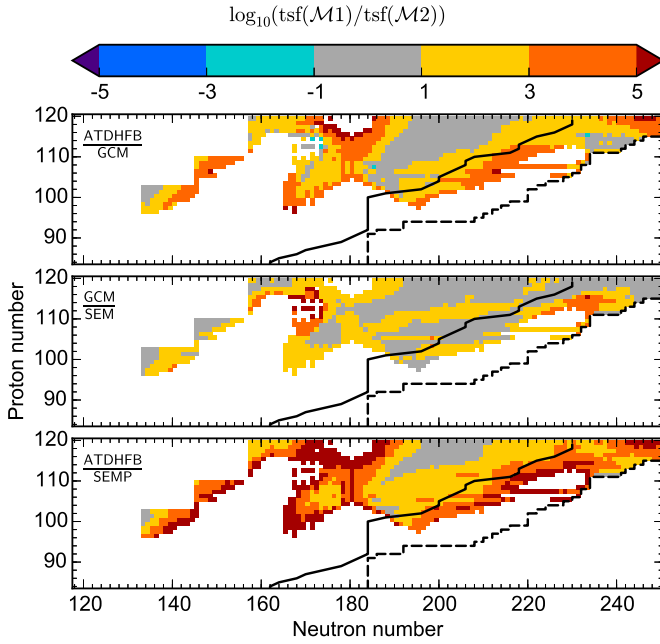


FIG. 10. Logarithm of the ratio of the spontaneous fission lifetimes for different combinations of collective inertias: $R_{\text{GCM}}^{\text{ATDHFB}}$ (upper panel); $R_{\text{SEMP}}^{\text{GCM}}$ (middle panel) and $R_{\text{SEMP}}^{\text{ATDHFB}}$ (lower panel).

D. α -decay half-lives

For completeness, we studied the competition between SF and α -decay. The α -decay half-lives are obtained by means of the Viola-Seaborg formula:

$$\log_{10}(t_{\alpha}[s]) = \frac{aZ + b}{\sqrt{Q_{\alpha}[\text{MeV}]}} + cZ + d + h_{\log}, \quad (17)$$

being Z the proton number of the parent nucleus. The Q_{α} value is obtained from the binding energies of the alpha particle, parent and daughter nuclei:

$$Q_{\alpha}(Z, N) = Be(Z, N) - Be(Z - 2, N - 2) - Be(^4\text{He}). \quad (18)$$

with $Be(^4\text{He}) = -28.296$ MeV. The coefficients of Eq. (17) are obtained from the recent parametrization of Ref. [60]:

$$a = 1.64062, \quad b = -8.54399, \quad (19)$$

$$c = -0.19430, \quad d = -33.9054, \quad (20)$$

with the hindrance factor

$$h_{\log} = \begin{cases} 0, & \text{for } Z \text{ even and } N \text{ even;} \\ 0.8937, & \text{for } Z \text{ even and } N \text{ odd;} \\ 0.5720, & \text{for } Z \text{ odd and } N \text{ even;} \\ 0.9380, & \text{for } Z \text{ odd and } N \text{ odd.} \end{cases} \quad (21)$$

The main advantage of the Viola-Seaborg formula is that it only requires the Q_{α} value of the parent nucleus to

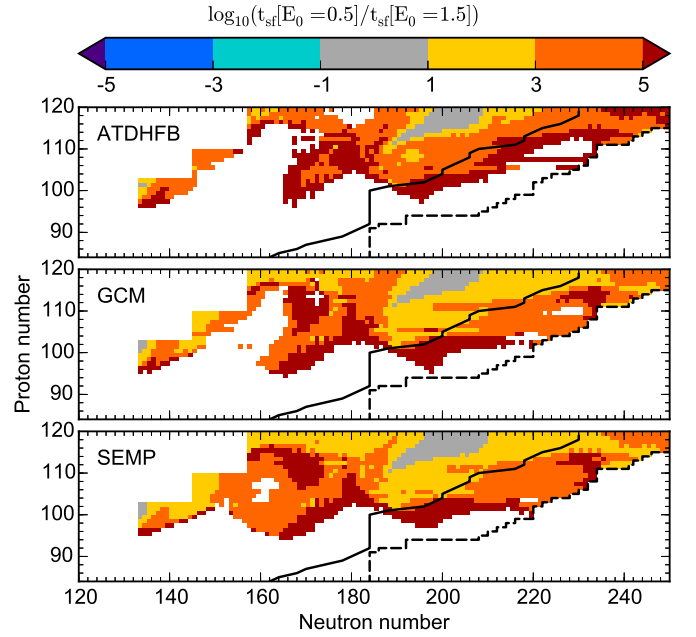


FIG. 11. Sensitivity of the spontaneous fission lifetimes to different values of the collective ground-state energy $\log_{10}[t_{\text{sf}}(E_0 = 0.5 \text{ MeV})/t_{\text{sf}}(E_0 = 1.5 \text{ MeV})]$ computed with different collective inertias: ATDHFB (upper panel), GCM (middle panel) and semiempirical inertia formula (lower panel).

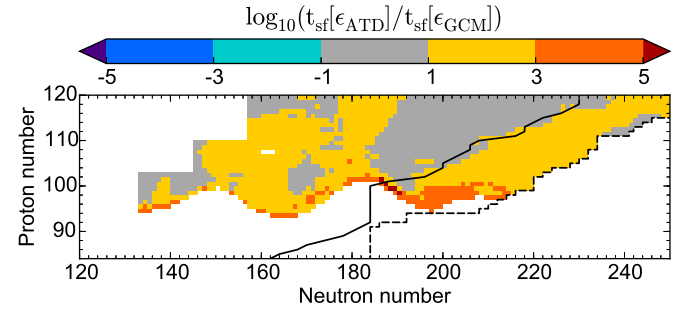


FIG. 12. Logarithm of the ratio of the spontaneous fission lifetimes of ATDHFB to GCM vibrational energy correction ϵ_{vib} computed using the semiempirical collective inertias.

compute the α -decay half-lives. Comparing our predictions with the AME2012 atomic mass evaluation [45], we found that BCPM reproduces the Q_{α} values with a rms deviation of 0.68 MeV. For the alpha decay half-lives of nuclei with $Z \geq 84$, the logarithm of the mean and standard deviations are 1.92 and 2.51 respectively, corresponding to deviations between theoretical half-lives and experimental data of factors 316 and 80. These large deviations in the t_{α} reflect the difficulties of reaching accuracies beyond the logarithmic precision in lifetimes calculations involving tunneling processes, as it was already mentioned in Sec. III A. Actually the accuracy of the Viola-Seaborg formula itself is larger than a factor 6 [60], and it is important to notice that the deviations obtained in the t_{α} are smaller than those obtained in the

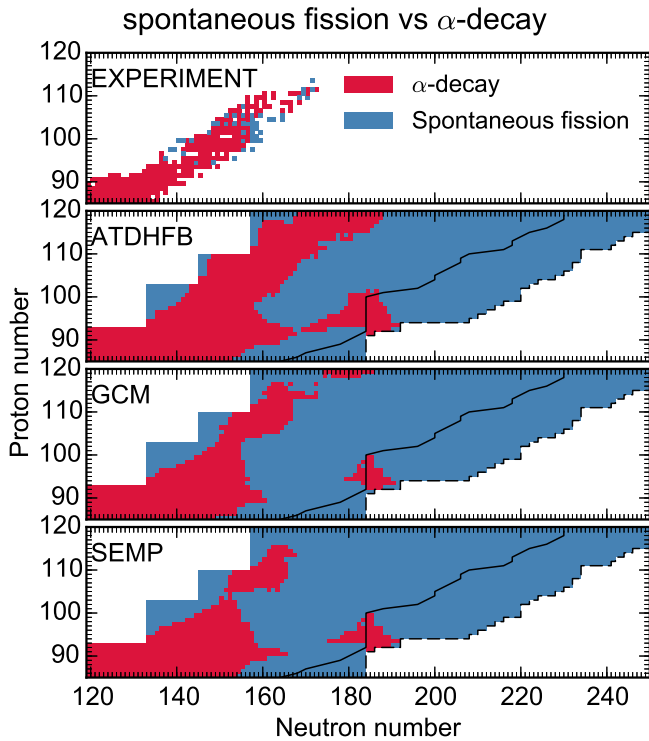


FIG. 13. Dominating channel between α -decay and spontaneous fission for different collective inertias. For comparison, the upper panel shows the dominating channel for nuclei experimentally observed [45].

t_{sf} without renormalization of the collective inertias.

Fig. 13 shows the dominating channel (either SF or α -decay) predicted by BCPM using different collective inertias, and the upper panel shows the experimental data extracted from Ref. [45]. All the inertia schemes predict α -decay to be the dominating channel in the region $84 \leq Z \leq 98$ and $118 \leq N \leq 156$, in good agreement with experimental data. However, only the ATDHFB and GCM schemes succeed in reproducing the α -decay path that starting from the lighter region proceeds towards $Z/N = 110/172$. This path forms the peninsula of stability already discussed in Sec. III B. In this region the semiempirical formula seems to underestimate the stability against the SF process, and the α -decay path is interrupted by the SF already at $A = 254$. One should also notice that the increasing stability around the predicted magic neutron number $N = 184$ produces an island of nuclei dominated by α -decay around $Z = 94$. Finally, the ATDHFB is the only scheme predicting the α -decay to be the dominating channel of most of the nuclei in the island of stability.

E. neutron induced rates

We conclude our study showing the impact of collective inertias on the calculations of rates relevant for r -process nucleosynthesis. Following the statistical picture

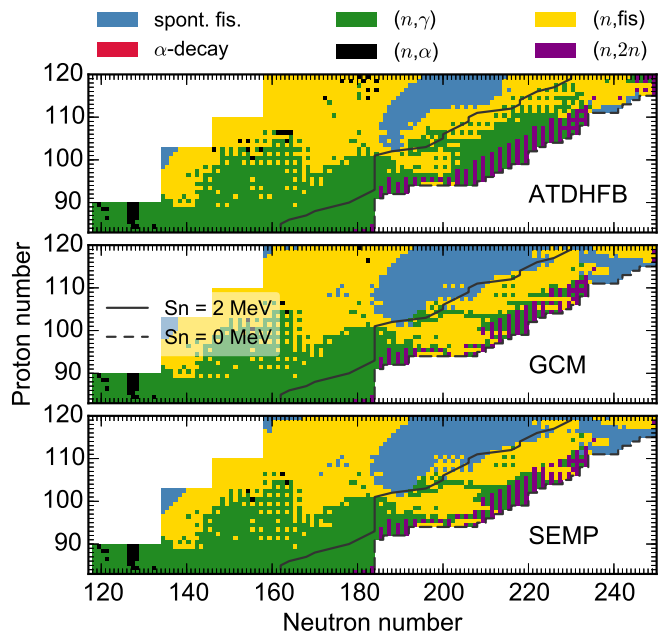


FIG. 14. Dominating decay channels: spontaneous fission, α -decay, neutron-capture, neutron-induced α emission, neutron-induced fission and two-neutron emission computed using different collective inertia schemes.

described by the Hauser-Feshbach theory, we computed the neutron capture, neutron induced fission, neutron induced α decay and neutron induced two-neutron emission stellar rates over the whole superheavy landscape using the binding energies, fission barriers and the non-renormalized collective inertias obtained from BCPM EDF. We adopted the level densities given by the Back-Shifted Fermi Gas Model and the Kopecky-Uhl generalized Lorentzian gamma-ray strengths [51]. The calculations were carried out using the TALYS reaction code [61] for a range of temperatures between 0.01 and 10 GK. Fig. 14 shows the dominating decay channel of each nucleus for typical conditions of r -process in neutron star mergers ($T = 0.9$ GK, $n_n = 1.0 \times 10^{28} \text{ cm}^{-3}$) [6]. Comparing the rates obtained from the different collective inertias, we found that the GCM and semiempirical schemes predict a rather similar scenario, while the ATDHFB differs in the region between the neutron dripline and the r -process path where this scheme predicts the neutron capture to dominate over fission decays. However, the material may never reach the narrow corridor in which (n, γ) dominates over (n, f) due to the even larger $(n, 2n)$ rates. We conclude then that independently of the computational scheme the production of nuclei heavier than $N > 184$ will be strongly hindered due to the dominance of neutron induced fission.

IV. CONCLUSIONS

We have presented fission properties of 3640 superheavy nuclei obtained within the Self-Consistent Mean-

Field scheme and the BCPM EDF. The fission path is computed by minimizing the potential energy using the axial quadrupole moment operator as a collective degree of freedom and allowing for octupole and hexadecapole deformations. The potential energy surface of nuclei with an odd number of protons and/or neutrons is calculated using the PNAM, maintaining the level of accuracy obtained for even-even nuclei. The spontaneous fission lifetimes are evaluated using the WKB formula involving the effective potential, collective inertias and collective ground-state energy of the nucleus. Both vibrational and rotational corrections are properly subtracted from the effective potential. Collective inertias are evaluated using three different schemes (ATDHFB, GCM and the semiempirical formula) to test the sensitivity of the spontaneous fission lifetimes.

Comparing our results with the available experimental data we found that BCPM tends to overestimate the spontaneous fission lifetimes, specially in the region of light actinides where the fission barriers and collective inertias are extremely large. In order to decrease this overestimation we propose a phenomenological approach based in the renormalization of the collective inertias, where the agreement with experiment can be improved by multiplying the collective inertias by constant factors. The comparison with experimental lifetimes showed that the accuracy and precision of the theoretical predictions improve as the mass number increases, providing the confidence to explore the region of nuclei relevant for the r -process.

The landscape of the fission barrier obtained with the BCPM EDF show five islands of local maxima. Both the magic neutron numbers 126 and 184 lead to an increase of the fission barriers. Two other regions of enhanced barriers are found corresponding to the peninsula and island of stability. BCPM predicts a region of vanishing barriers for nuclei with $A \sim 292$, in agreement with other theoretical models. By studying the energy window of the neutron induced fission, we concluded that the r -process path may terminate in this region and cycle to lighter fission products.

We performed a complete study of the sensitivity of the spontaneous fission lifetimes to the quantities entering in the WKB formula. We studied the variations on lifetimes when different schemes of the collective inertias, vibrational energy corrections and collective ground-state energies are used. For r -process nuclei, different collective inertia schemes result in differences in the spontaneous fission lifetimes between one and three orders of

magnitude. The ATDHFB scheme predicts systematically larger lifetimes than GCM, while the semiempirical schemes has the lower t_{sf} . We also found that the spontaneous fission lifetimes are strongly affected by the collective ground-state energy E_0 . These large variations on the lifetimes can be related to a complex structure of the fission paths where several humps are present. Some of the barriers and isomers are placed 0.6–1.2 MeV above the ground state and their contribution to the action integral strongly depends on the value of E_0 . On the other hand, variations of the lifetimes on different schemes of the vibrational corrections are found to be small compared to the ones discussed above.

Finally, we studied the competition of fission with other channels. We computed the α -decay half-lives by means of the Viola-Seaborg formula and compared the results with the spontaneous fission lifetimes. We found that for both the ATDHFB and GCM schemes the α -decay dominates in a continuous path around $N-Z = 50$, in a rather good agreement with experimental data, while the semiempirical inertias predict a corridor around $Z/N = 104/156$ where fission dominates. Using the statistical approach we computed neutron induced rates based on binding energies, fission barriers and the non-normalized collective inertias obtained from the BCPM EDF. Our calculations showed that independently of the computational scheme adopted the production of nuclei above $N > 184$ will be strongly inhibited by the neutron induced fission.

The impact of collective inertias on neutron induced rates suggests that the r -process abundances could be sensitive to this quantity. Additionally, the calculation of beta delayed fission rates is necessary in order to perform r -process calculations. Work along these lines is already in progress.

ACKNOWLEDGMENTS

The authors are grateful to Hans Feldmeier for his helpful discussions on theoretical aspects of the fission process and to Stephane Goriely for providing the HFB14 fission barriers plotted in Fig. 7. SAG and GMP acknowledge support from the Deutsche Forschungsgemeinschaft through contract SFB 1245, and the BMBF-Verbundforschungsprojekt number 05P15RDFN1. The work of L. M. Robledo has been supported in part by the Spanish MINECO Grants No. FPA2012-34694 and No. FIS2012-34479 and by the ConsoliderIngenio 2010 Program MULTIDARK CSD2009-00064.

-
- [1] J. J. Cowan, F.-K. Thielemann, and J. W. Truran, *Phys. Rep.* **208**, 267 (1991).
 - [2] G. Martínez-Pinedo, D. Mocerj, N. T. Zinner, A. Kelić-Heil, K. Langanke, I. V. Panov, B. Pfeiffer, T. Rauscher, K.-H. Schmidt, and F.-K. Thielemann, *Prog. Part. Nucl. Phys.* **59**, 199 (2007).
 - [3] S. Goriely, *Eur. Phys. J. A* **51** (2015), 10.1140/epja/i2015-15022-3.
 - [4] S. Goriely, J.-L. Sida, J.-F. Lemaître, S. Panebianco, N. Dubray, S. Hilaire, A. Bauswein, and H.-T. Janka, *Phys. Rev. Lett.* **111**, 242502 (2013).
 - [5] M. Eichler, A. Arcones, A. Kelic, O. Korobkin, K. Lan-

- ganke, T. Marketin, G. Martínez-Pinedo, I. V. Panov, T. Rauscher, S. Rosswog, C. Winteler, N. T. Zinner, F.-K. Thielemann, A. Kelić-Heil, O. Korobkin, K. Langanke, T. Marketin, G. Martínez-Pinedo, I. V. Panov, T. Rauscher, S. Rosswog, C. Winteler, N. T. Zinner, and F.-K. Thielemann, *Astrophys. J.* **808**, 30 (2015).
- [6] J. J. Mendoza-Temis, M.-R. Wu, K. Langanke, G. Martínez-Pinedo, A. Bauswein, and H.-T. Janka, *Phys. Rev. C* **92**, 055805 (2015).
- [7] L. Stavsetra, K. E. Gregorich, J. Dvorak, P. A. Ellison, I. Dragojević, M. A. Garcia, and H. Nitsche, *Phys. Rev. Lett.* **103**, 132502 (2009).
- [8] C. E. Düllmann, M. Schädel, A. Yakushev, A. Türler, K. Eberhardt, J. V. Kratz, D. Ackermann, L.-L. Andersson, M. Block, W. Brühle, J. Dvorak, H. G. Essel, P. A. Ellison, J. Even, J. M. Gates, A. Gorshkov, R. Graeger, K. E. Gregorich, W. Hartmann, R.-D. Herzberg, F. P. Heßberger, D. Hild, A. Hübner, E. Jäger, J. Khuyagbaatar, B. Kindler, J. Krier, N. Kurz, S. Lahiri, D. Liebe, B. Lommel, M. Maiti, H. Nitsche, J. P. Omtvedt, E. Parr, D. Rudolph, J. Runke, B. Schausten, E. Schimpf, A. Semchenkov, J. Steiner, P. Thörle-Pospiech, J. Uusitalo, M. Wegrzecki, and N. Wiehl, *Phys. Rev. Lett.* **104**, 252701 (2010).
- [9] Y. T. Oganessian, F. S. Abdullin, C. Alexander, J. Binder, R. A. Boll, S. N. Dmitriev, J. Ezold, K. Felker, J. M. Gostic, R. K. Grzywacz, J. H. Hamilton, R. A. Henderson, M. G. Itkis, K. Miernik, D. Miller, K. J. Moody, A. N. Polyakov, A. V. Ramayya, J. B. Roberto, M. A. Ryabinin, K. P. Rykaczewski, R. N. Sagaidak, D. A. Shaughnessy, I. V. Shirokovsky, M. V. Shumeiko, M. A. Stoyer, N. J. Stoyer, V. G. Subbotin, A. M. Sukhov, Y. S. Tsyganov, V. K. Utyonkov, A. A. Voinov, and G. K. Vostokin, *Phys. Rev. Lett.* **109**, 162501 (2012).
- [10] J. Khuyagbaatar, A. Yakushev, C. E. Düllmann, D. Ackermann, L.-L. Andersson, M. Asai, M. Block, R. A. Boll, H. Brand, D. M. Cox, M. Dasgupta, X. Derkx, A. Di Nitto, K. Eberhardt, J. Even, M. Evers, C. Fahlander, U. Forsberg, J. M. Gates, N. Gharibyan, P. Golubev, K. E. Gregorich, J. H. Hamilton, W. Hartmann, R.-D. Herzberg, F. P. Heßberger, D. J. Hinde, J. Hoffmann, R. Hollinger, A. Hübner, E. Jäger, B. Kindler, J. V. Kratz, J. Krier, N. Kurz, M. Laatiaoui, S. Lahiri, R. Lang, B. Lommel, M. Maiti, K. Miernik, S. Minami, A. Mistry, C. Mokry, H. Nitsche, J. P. Omtvedt, G. K. Pang, P. Papadakis, D. Renisch, J. Roberto, D. Rudolph, J. Runke, K. P. Rykaczewski, L. G. Sarmiento, M. Schädel, B. Schausten, A. Semchenkov, D. A. Shaughnessy, P. Steinegger, J. Steiner, E. E. Tereshatov, P. Thörle-Pospiech, K. Tinschert, T. Torres De Heidenreich, N. Trautmann, A. Türler, J. Uusitalo, D. E. Ward, M. Wegrzecki, N. Wiehl, S. M. Van Cleve, and V. Yakusheva, *Phys. Rev. Lett.* **112**, 172501 (2014).
- [11] A. Baran, M. Kowal, P.-G. Reinhard, L. M. Robledo, A. Staszczak, and M. Warda, *Nucl. Phys. A* **944**, 442 (2015).
- [12] P. Jachimowicz, M. Kowal, and J. Skalski, *Phys. Rev. C* **92**, 044306 (2015).
- [13] P. Möller, A. J. Sierk, T. Ichikawa, A. Iwamoto, and M. R. Mumpower, *Phys. Rev. C* **91**, 024310 (2015).
- [14] P. Jachimowicz, M. Kowal, and J. Skalski, *Phys. Rev. C* **95**, 014303 (2017).
- [15] S. Goriely, M. Samyn, and J. M. Pearson, *Phys. Rev. C* **75**, 064312 (2007).
- [16] S. Goriely, S. Hilaire, A. J. Koning, M. Sin, and R. Capote, *Phys. Rev. C* **79**, 024612 (2009).
- [17] J. C. Pei, W. Nazarewicz, J. A. Sheikh, and A. K. Kerman, *Phys. Rev. Lett.* **102**, 192501 (2009).
- [18] J. A. Sheikh, W. Nazarewicz, and J. C. Pei, *Phys. Rev. C* **80**, 30 (2009).
- [19] J. Erler, K. Langanke, H. P. Loens, G. Martínez-Pinedo, and P.-G. Reinhard, *Phys. Rev. C* **85**, 025802 (2012).
- [20] A. Staszczak, A. Baran, and W. Nazarewicz, *Phys. Rev. C* **87**, 024320 (2013).
- [21] J. Sadhukhan, W. Nazarewicz, and N. Schunck, *Phys. Rev. C* **93**, 011304 (2016).
- [22] M. Warda, J. L. Egido, L. M. Robledo, and K. Pomorski, *Phys. Rev. C* **66**, 014310 (2002).
- [23] M. Warda and L. M. Robledo, *Phys. Rev. C* **84**, 44608 (2011).
- [24] J.-P. Delaroche, M. Girod, H. Goutte, and J. Libert, *Nucl. Phys. A* **771**, 103 (2006).
- [25] M. Warda and J. L. Egido, *Phys. Rev. C* **86**, 014322 (2012).
- [26] R. Rodríguez-Guzmán and L. M. Robledo, *Phys. Rev. C* **89**, 054310 (2014).
- [27] R. Rodríguez-Guzmán and L. M. Robledo, *Eur. Phys. J. A* **50**, 142 (2014).
- [28] R. Rodríguez-Guzmán and L. M. Robledo, *Eur. Phys. J. A* **52**, 12 (2016).
- [29] B. N. Lu, J. Zhao, E. G. Zhao, and S.-G. Zhou, *Phys. Rev. C* **89**, 1 (2014).
- [30] N. Schunck and L. M. Robledo, *Reports Prog. Phys.* **79**, 116301 (2016).
- [31] M. Baldo, L. M. Robledo, P. Schuck, and X. Viñas, *Phys. Rev. C* **87**, 064305 (2013).
- [32] S. Goriely and G. Martínez-Pinedo, *Nucl. Phys. A* **1**, 1 (2015).
- [33] M. Bender, P.-H. Heenen, and P.-G. Reinhard, *Rev. Mod. Phys.* **75**, 121 (2003).
- [34] S. A. Giuliani and L. M. Robledo, *Phys. Rev. C* **88**, 054325 (2013).
- [35] J. Sadhukhan, J. Dobaczewski, W. Nazarewicz, J. A. Sheikh, and A. Baran, *Phys. Rev. C* **90**, 1 (2014).
- [36] J. Zhao, B.-N. Lu, T. Nikšić, D. Vretenar, and S.-G. Zhou, *Phys. Rev. C* **93**, 044315 (2016).
- [37] L. M. Robledo and G. F. Bertsch, *Phys. Rev. C* **84**, 14312 (2011).
- [38] S. A. Giuliani, L. M. Robledo, and R. Rodríguez-Guzmán, *Phys. Rev. C* **90**, 054311 (2014).
- [39] M. Brack, J. Damgaard, A. Jensen, H. Pauli, V. Strutinsky, C. Wong, and A. S. Jen, *Rev. Mod. Phys.* **44**, 320 (1972).
- [40] A. Baran, K. Pomorski, A. Lukasiak, and A. Sobczewski, *Nucl. Phys. A* **361**, 83 (1981).
- [41] J. L. Egido and L. M. Robledo, in *Ext. Density Funct. Nucl. Struct. Phys.*, Vol. 641 (2004) pp. 269–302.
- [42] M. Girod and B. Grammaticos, *Nucl. Phys. A* **330**, 40 (1979).
- [43] P. Ring and P. Schuck, (1980) pp. 1–718.
- [44] S. G. Nilsson, J. R. Nix, A. Sobczewski, Z. Szymański, S. Wycech, C. Gustafson, and P. Möller, *Nucl. Phys. A* **115**, 545 (1968).
- [45] M. Wang, G. Audi, A. H. Wapstra, F. Kondev, M. Maccormick, X. Xu, and B. Pfeiffer, *Chinese Phys. C* **36**, 1603 (2012).
- [46] L. M. Robledo, R. Bernard, and G. F. Bertsch, *Phys. Rev. C* **86**, 064313 (2012).
- [47] T. Duguet, P. Bonche, P.-H. Heenen, and J. Meyer, *Phys. Rev. C* **65**, 014310 (2001).

- [48] S. Goriely, N. Chamel, and J. M. Pearson, *Phys. Rev. C* **82**, 035804 (2010).
- [49] P. Möller, J. R. Nix, W. Myers, and W. Swiatecki, *At. Data Nucl. Data Tables* **59**, 185 (1995).
- [50] S. Bjørnholm and J. E. Lynn, *Rev. Mod. Phys.* **52**, 725 (1980).
- [51] R. Capote, M. Herman, P. Obložinský, P. G. Young, S. Goriely, T. Belgia, V. Ignatyuk, A. J. Koning, S. Hilaire, V. Plujko, M. Avrigeanu, O. Bersillon, M. B. Chadwick, T. Fukahori, Z. Ge, Y. Han, S. Kailas, J. Kopecky, V. M. Maslov, G. Reffo, M. Sin, E. Soukhovitskii, and P. Talou, *Nucl. Data Sheets* **110**, 3107 (2009).
- [52] N. E. Holden and D. C. Hoffman, *Pure Appl. Chem.* **72**, 1525 (2000).
- [53] J. Khuyagbaatar, S. Hofmann, F. P. Heßberger, D. Ackermann, H. G. Burkhard, S. Heinz, B. Kindler, I. Kojouharov, B. Lommel, R. Mann, J. Maurer, K. Nishio, and Y. Novikov, *Eur. Phys. J. A* **37**, 177 (2008).
- [54] A. Baran, J. A. Sheikh, J. Dobaczewski, W. Nazarewicz, and A. Staszczak, *Phys. Rev. C* **84**, 054321 (2011).
- [55] G. F. Bertsch, W. Loveland, W. Nazarewicz, and P. Talou, *J. Phys. G Nucl. Part. Phys.* **42**, 077001 (2015).
- [56] G. Audi, A. H. Wapstra, and C. Thibault, *Nucl. Phys. A* **729**, 337 (2003).
- [57] G. Martínez-Pinedo, *Eur. Phys. J. Spec. Top.* **156**, 123 (2008).
- [58] I. V. Panov, I. Y. Korneev, T. Rauscher, G. Martínez-Pinedo, A. Kelić-Heil, N. T. Zinner, and F.-K. Thielemann, *Astron. Astrophys.* **513**, 14 (2010).
- [59] I. Petermann, K. Langanke, G. Martínez-Pinedo, I. V. Panov, P.-G. Reinhard, and F.-K. Thielemann, *Eur. Phys. J. A* **48**, 122 (2012).
- [60] T. Dong and Z. Ren, *Eur. Phys. J. A* **26**, 69 (2005).
- [61] A. J. Koning, S. Hilaire, and S. Goriely, “*Talys 1.8 user manual*,” (2015).